Nuclear Engineering and Technology 53 (2021) 888–893

Contents lists available at ScienceDirect

Nuclear Engineering and Technology

journal homepage: www.elsevier.com/locate/net

Original Article

Development of de-noised image reconstruction technique using Convolutional AutoEncoder for fast monitoring of fuel assemblies

Se Hwan Choi [a], Hyun Joon Choi [b], Chul Hee Min [b], Young Hyun Chung [b], Jae Joon Ahn [a, *]

[a] Department of Information and Statistics, Yonsei University, Republic of Korea
[b] Department of Radiation Convergence Engineering, Yonsei University, Republic of Korea

ARTICLE INFO

Article history:
Received 28 April 2020
Received in revised form
5 August 2020
Accepted 24 August 2020
Available online 28 August 2020

Keywords:
Tomographic imaging
Verification of fuel assemblies
Deep learning-based denoising process
Convolutional autoencoder

ABSTRACT

The International Atomic Energy Agency has developed a tomographic imaging system for accomplishing the total fuel rod-by-rod verification time of fuel assemblies within the order of 1–2 h, however, there are still limitations for some fuel types. The aim of this study is to develop a deep learning-based de-noising process resulting in increasing the tomographic image acquisition speed of fuel assembly compared to the conventional techniques. Convolutional AutoEncoder (CAE) was employed for de-noising the low-quality images reconstructed by filtered back-projection (FBP) algorithm. The image data set was constructed by the Monte Carlo method with the FBP and ground truth (GT) images for 511 patterns of missing fuel rods. The de-noising performance of the CAE model was evaluated by comparing the pixel-by-pixel subtracted images between the GT and FBP images and the GT and CAE images; the average differences of the pixel values for the sample image 1, 2, and 3 were 7.7%, 28.0% and 44.7% for the FBP images, and 0.5%, 1.4% and 1.9% for the predicted image, respectively. Even for the FBP images not discriminable the source patterns, the CAE model could successfully estimate the patterns similarly with the GT image.

1. Introduction

Single-photon emission tomography (SPECT) technique is a nuclear medicine tomographic imaging technique generally used in the clinic to obtain three-dimensional (3-D) information of a gamma-emitting radioisotope distribution in the patient. This technique has been applied to various industrial research fields for the purpose of non-destructive analysis (NDA) for environmental monitoring or safeguards.

The International Atomic Energy Agency (IAEA) has always paid due attention to the development of safeguards techniques for irradiated-fuel storage and has monitored the amount of nuclear materials of each country for managing and supervising peaceful nuclear activities [1]. For the quantitative verification of the amount of nuclear material presented in the State's accounts, over a hundred different types of NDA equipment have been developed for many years [2]; however, they still have limitations in detecting whether a fraction of a declared amount of nuclear material is missing owing to its high detection uncertainty and volume averaging assessment. Therefore, SPECT technique has considered as one of the most attractive techniques for safeguards of a spent fuel assembly owing to its capability of intuitive distinction of missing fuel pellets or fuel rods. The IAEA has developed SPECT imaging system from 2004 and various types of imaging systems have been proposed [3–6]. The IAEA aims to reduce the total verification time of unirradiated fuel assemblies within the order of 1–2 h; however, it could be up to 10 h for some fuel types by using the most recently developed SPECT system [6].

Unlike a human body, the spent fuel assembly is composed of high Z materials; therefore which results in degrading the projection image quality because of the high probability of attenuation and scatter of gamma rays by high Z materials. Furthermore, the image quality depends on the collimator geometry of the SPECT system. One of the methods for reducing verification time is to develop an image quality improvement technique because there is a tradeoff between image acquisition speed and image quality.

Filtered back-projection (FBP) algorithm is the most simple and fast image reconstruction algorithm applying a convolution filter to remove blurring; however, image reconstruction performance of this algorithm is sensitive to source quality or gamma detection performance. Compared with FBP, iterative reconstruction

* Corresponding author.
E-mail address: ahn2615@yonsei.ac.kr (J.J. Ahn).

https://doi.org/10.1016/j.net.2020.08.020

algorithm can improve image quality through a procedure iteratively comparing between images assumed by a statistical model and real-time measured values; however, it needs a lot of computational costs and an optimization process of the number of iteration and analytical model. Recently, deep learning (DL)-based image processing has been actively investigated and proved to outperform other techniques in improving image quality. This technique enables to obtain de-noised images within a very short time from low-quality images by training a DL algorithm about complex relationships between the high-quality images and low-quality images. Many researchers have shown its remarkable performance in the de-noising research area by using various DL models.

AutoEncoders are a type of generative model used for unsupervised learning and a Simple AutoEncoder (SAE) is an easily useable model showing high performance in removing blurring on an image [7]. A Convolutional AutoEncoder (CAE) was recently introduced that converted the hidden layer of SAE from neural networks to convolution layer. The CAE model shows the better performance in de-noising compared with SAE model [8], because the convolution layer has better image recognition than neural networks. Several studies using the CAE model for thermal images [9] and medical imaging analysis [10] also showed great performance of the CAE model.

The aim of this study is to develop a CAE model-based de-noised image reconstruction technique resulting in increasing the tomographic image acquisition speed of fuel assembly compared to the conventional techniques to reduce the total verification time. In this study, we trained a CAE model for various patterns of fuel rods in a 3×3 array assembly structure and evaluated the de-noising performance for various quality of FBP images.

2. Materials and methods

2.1. Tomographic image acquisition of fuel assembly

In our previous study, we designed a dual-head SPECT system using Monte Carlo (MC) method in GATE (v. 8.1) [11]. The detector head of the SPECT system is composed of $0.3 \times 4 \times 4$ (front side) and 0.3 (back side) cm^3 trapezoidal BGO scintillators and $0.2 \times 5 \times 4$ cm^3 slits surrounded by tungsten materials in front of each scintillator; located in every 0.4 cm intervals. Field-of-view of the detector was 25.6×4 cm^2 and the surface of the detector was 22 cm apart from the center of a fuel assembly, which consists of 3×3 fuel rod array where the diameter of fuel rod locating in every 1.269 cm intervals is 0.994 cm. Fuel source was assumed as a spent fuel burned up of 10327 MWd/MTU and cooled for 5 years; the major radionuclide of the spent fuel is Cs-137 because of its long half-life (about 30 years). In the 3×3 array of the fuel assembly, total of 511 patterns of missing fuel rods are possible and the 128×128 tomographic images for these patterns were reconstructed by FBP algorithm using 400 projection data acquired during 360° rotation. For obtaining projection data for 64 channels of the detector head, the total detection count for a 400–700 keV energy window in an energy spectrum deposited in the BGO scintillator of each channel was used for data processing.

2.2. Ground truth image generation

A ground truth (GT) image shows the actual pattern of fuel rods in the assembly regarding the low-quality FBP image. The GT images for 511 patterns were generated based on geometrical information of the fuel assembly. The fuel rod consists of UO_2 (10.519 g/cm^3), ZIRLO (6.578 g/cm^3) and He gas (2.222 mg/cm^3). Averaged electron density for these materials relative to that of water was assigned in each pixel of 128×128 virtual grid based on detailed geometrical information of fuel rod and assembly. This GT image generated based on the electron density of each material can be used for the attenuation and scatter correction on the reconstructed image. Source activity distribution of fuel assembly set in GATE simulation can be assigned on the GT image. The GT image and FBP image sets were used for training the deep learning-based image reconstruction algorithm using CAE.

2.3. Convolutional AutoEncoder-based de-noising technique

Convolution neural networks (CNN) consists of convolution, activation function, and pooling layer as a method of image recognition [12,13]. The convolution layer splits the input image into small subsets and extracts multiple features using a filter from the input image [13]; this is similar to the process by which people perceive things. In general, the activation function uses a non-linear function to express hidden relationships. Fig. 1 shows the computational process of CNN. In the convolution layer, the convolved map are extracted by using a filter where the size of 3×3. After then, Relu function, the activation function, is applied to the convolved map and a feature map is generated. The Relu function helps for the gradient vanishing problem and makes the training speed to increase [14]. In the max-pooling layer, the feature map is scanned by a 2×2 max-pooling filter with a similar procedure illustrated in Fig. 1. After then, the biggest pixel value of the feature map is extracted on the overlapped region between the feature map and the max-pooling filter. Based on this procedure, the size of the image is reduced by half.

Fig. 2 shows a schematic diagram of the CAE model. The CAE model is a combination model of the CNN model and AutoEncoder [15,16]. The AutoEncoder consists of an encoder and a decoder. The encoder extracts characteristics of the input image by reducing the dimension of the image, and then the decoder reconstructs the transformed image with increasing the dimension based on features extracted from the encoder [16]. In the CAE model, the encoder is composed of two convolution layers where the filter size is 3×3 and two max-pooling layers where the pooling size is 2×2, and these layers are positioned alternatively. The first convolution layer extracts multiple features using 32 filters and the size of the input image is reduced by half in the first max-pooling layer. The second convolution layer also extracts features using 64 filters and the second max-pooling layer reduces the size of the image by half again and generates 64 feature maps where the size of 32×32. The decoder is composed of the same convolution layers in the opposite structure to the encoder and two up-sampling layers where the up-sampling size is 2×2. The first convolution layer in the decoder takes the 64 feature maps generated in encoder using 64 filters and the map dimension is increased by twice in the first up-sampling layer. The second convolution layer having 32 filters and up-sampling layer perform the same procedure and generates 32 feature maps where the size of 128×128. Like the CNN, the Relu function was applied as the activation function to both encoder and decoder. Finally, the output image was obtained by applying the convolution layer having one filter to the feature maps extracted from the decoder. In this final procedure, the activation function of the convolution layer was set to a sigmoid function, where the minimum and maximum values are 0 and 1, respectively, to estimate the probability of the pixel.

A loss function that is able to evaluate the difference between the output image generated through the CAE model and the GT image was set to mean squared error (MSE). MSE is one of the most generally used loss functions for evaluating the accuracy of the DL model. The CAE model was optimized by minimizing the pixel-by-

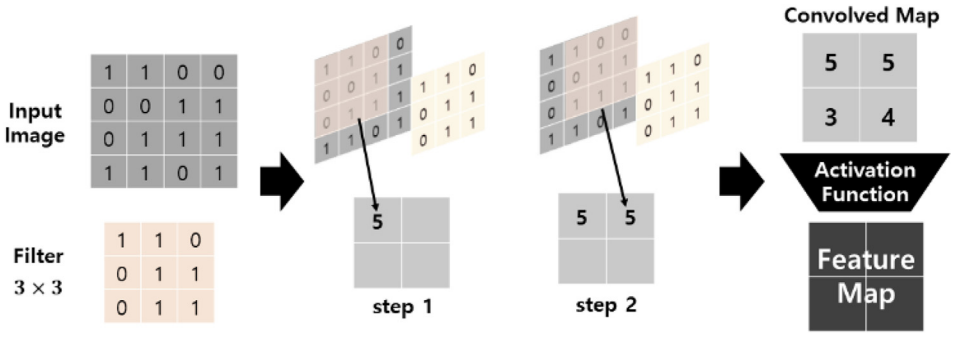

Fig. 1. Feature map generating process of convolution neural networks.

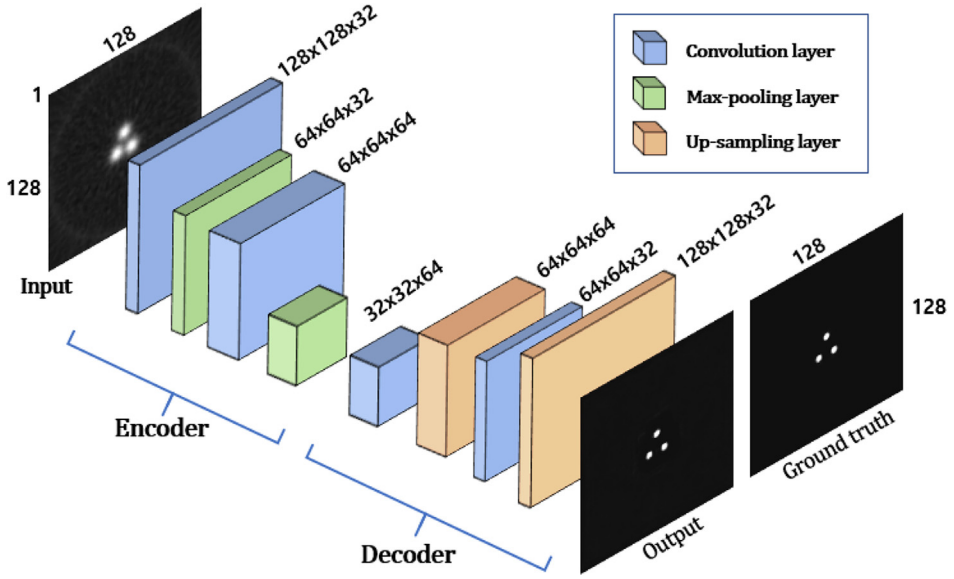

Fig. 2. Schematic diagram of the structure of the Convolutional AutoEncoder.

pixel difference using Eq (1), where GT_{nhv} and CAE_{nhv} are pixel values of GT and CAE images, respectively, regarding nth pattern of missing fuel rods, hth position on the x-axis of the image, and vth position on the y-axis of the image. The optimization method was set to Adam having an efficient order of computation and stable optimization in image recognition.

$$MSE = \frac{1}{N}\frac{1}{H}\frac{1}{V}\sum_{n}^{N}\sum_{h}^{H}\sum_{v}^{V}(GT_{nhv} - CAE_{nhv})^2 \quad (1)$$

2.4. De-noising performance evaluation of the CAE model for various qualities of tomographic images

Among 511 GT-FBP image sets, 501 image sets were used for training the CAE model and the rest of the image sets were used for evaluating the de-noising performance of the CAE model. To quantitatively evaluate the de-noising performance, the average difference of pixel values in a specific region of interest for the 3 × 3 array of the fuel assembly was calculated between GT and FBP images and GT and CAE images. The source activity of the single fuel rod was set to 1.5 MBq, and we obtained four different quality of FBP images for 511 patterns of missing fuel rods by scanning the assembly for different times: 0.6, 10, 20, and 60 min. The performance of the CAE model was evaluated four times separately using four different quality of 511 GT-FBP image sets.

3. Results and discussion

3.1. Loss function

For training the CAE model, batch size, iteration, and epoch were set to 1, 501, and 100, respectively. These optimized hyperparameters were obtained by iteratively changing conditions and comparing image quality and computation performance. As the training of the CAE model proceeds, the MSE between the GT and CAE images decreases as illustrated in Fig. 3. When the epoch was 16 times, the MSE became almost zero and which was stably maintained until the end of the training; which means that the CAE model was successfully trained to estimate well the GT image from the FBP image. Meanwhile, as the number of epoch increasing, the computation cost also increases. Therefore, based on the analysis of this loss function, we could optimally determine the number of epoch for training well the CAE model.

3.2. De-noising performance of the Convolutional AutoEncoder

Fig. 4 illustrates the comparison of the GT, FBP, and CAE images for three sample patterns of missing fuel rods. Fig. 5 shows the

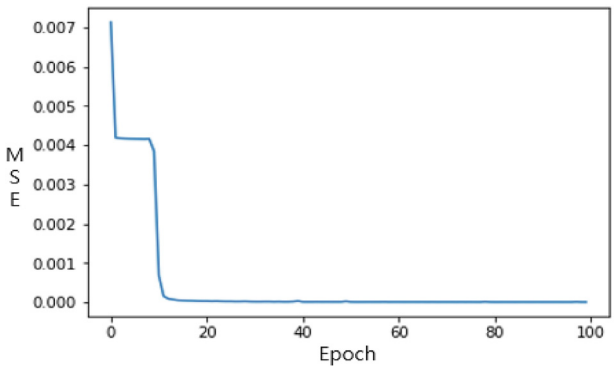

Fig. 3. Loss function curve showing the change of the mean squared error for the number of epoch.

comparison of the pixel-by-pixel subtracted images between the GT and FBP images and the GT and CAE images. As the results of the evaluation, the average differences of the pixel values of the region of interest (yellow box in Fig. 4) in the subtracted images for the sample 1, 2, and 3 were 7.7%, 28.0% and 44.7% for the FBP images, and 0.5%, 1.4% and 1.9% for the predicted image, respectively. The FBP images obtained by the dual-head SPECT system could successfully estimate the patterns of missing fuel rods because the image acquisition was performed in relatively ideal condition in GATE; the probabilities of the attenuation and scatter by the structure of the fuel assembly were small enough because of the small array size; the time for data acquisition was long enough (60 min); variations in the gamma detection efficiencies for the 64 channels of the detector were almost zero. However, the FBP images were quite blurry caused by the inherent spatial resolution of the detector. Furthermore, we could find ring artifacts on the FBP image caused by the limited number of projection images acquired during 360° rotation. On the other hand, the CAE images showed the de-noised high-quality images almost similar to the GT images, which enables the rod-by-rod discrimination. We expect that this CAE model is able to detect the small variation in the assembly through further research with more extensive big data constructed using more various source activity distribution and with the more detailed feature extraction techniques in the CAE model.

3.3. Application of the Convolutional AutoEncoder to the various FBP image qualities

Fig. 6 illustrates the comparison of the de-noising performance of the CAE model for four different FBP image qualities. As decreasing the time for scanning the assembly, the noise level increases, and the FBP images obtained by scanning for 0.6 min were not able to discriminate the pattern of missing fuel rods. However, even though some noises were revealed on the CAE images for the bad quality of the FBP image, the CAE models separately trained for four qualities of the FBP images could successfully estimate two patterns of missing fuel rods almost similarly with the GT images. When all the four kinds of 511 GT-FBP image sets were used for training the CAE model, it could successfully estimate the patterns for all image qualities, as well. In these results, we could see the possibility of reducing the image acquisition time about 10 times, and expect to be able to optimize the CAE model by determining a minimum estimable image quality in further research.

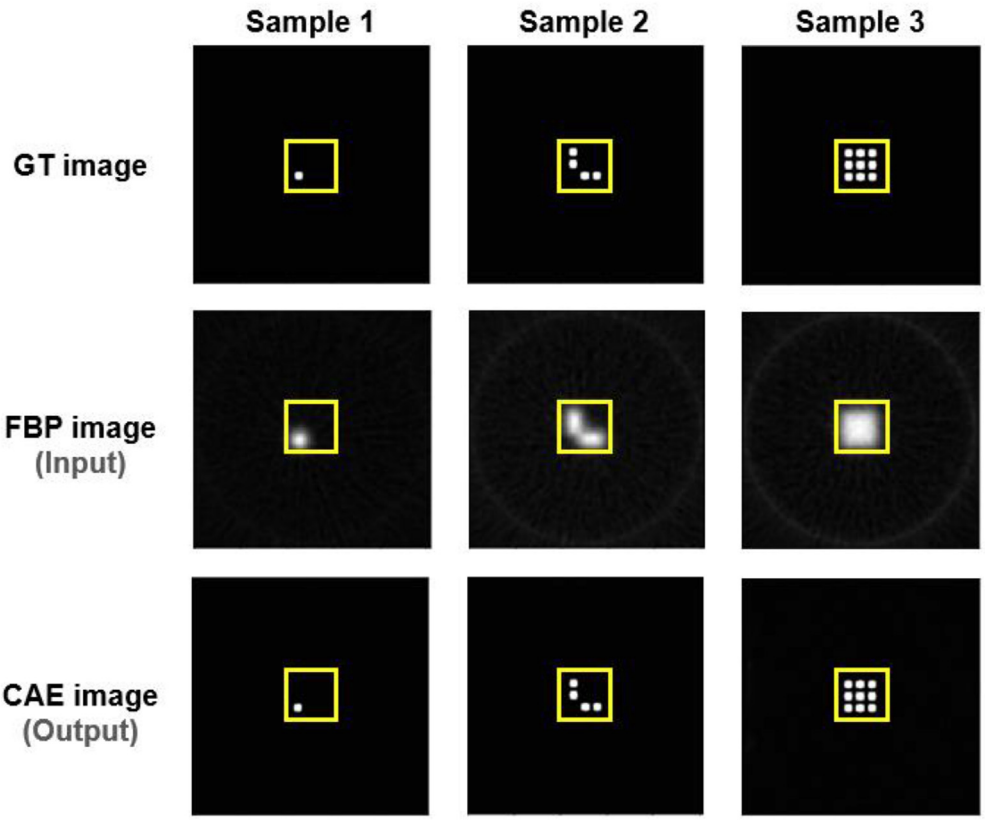

Fig. 4. Comparison of the GT, FBP, and CAE images for three sample patterns of missing fuel rods.

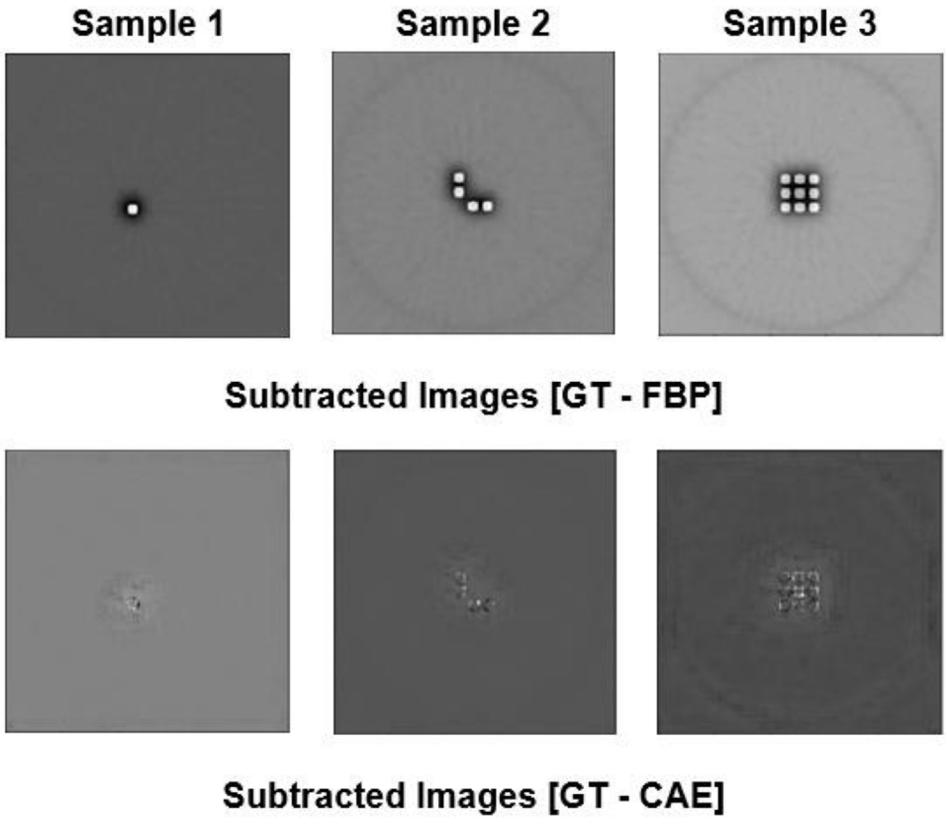

Fig. 5. Comparison of subtracted images between the GT and FBP images (upper) and the GT and CAE images (lower) for three sample patterns of missing fuel rods.

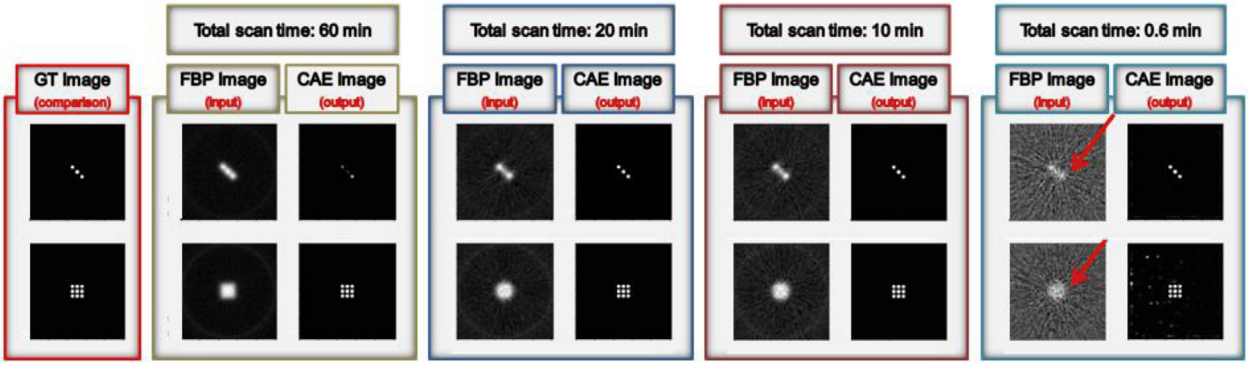

Fig. 6. Comparison of the de-noising performance of the CAE model for four different FBP image qualities obtained by scanning the assembly for 0.6, 10, 20, and 60 min.

4. Conclusion

In this study, the de-noised image reconstruction technique using the CAE model was developed for increasing the tomographic image acquisition speed to reduce the total verification time of the fuel assembly as following the IAEA recommendation. The results of this study showed the capability of the CAE model for a great improvement of the image quality from the FBP images almost similarly with the GT images. Even though the quality of the FBP image, input image of the CAE model, becomes bad, the CAE model could also discriminate the patterns of missing fuel rods similarly to when the image quality was the best. In the future, an optimization study of the CAE model will be performed to apply this model to experimentally obtained tomographic images of an unirradiated test fuel assembly installed in the Korea Institute of Nuclear Nonproliferation And Control. Also, additional experiments for applying proposed model to extended fuel assembly environments (e.g. 16×16 or 19×19 fuel assembly) will be conducted in further research.

Declaration of competing interest

The authors declare that they have no known competing financial interests or personal relationships that could have appeared to influence the work reported in this paper.

Acknowledgment

This research was supported by the Nuclear Safety Research Program through the Korea Foundation Of Nuclear Safety (KoFONS)

using the financial resource granted by the Nuclear Safety and Security Commission (NSSC) of the Republic of Korea (No. 1803027).

References

[1] S. Techniques, Equipment 2003 Edition, International Nuclear Verification Series No. 1 (Revised), IAEA, Vienna, 2003.
[2] M. Zendel, IAEA safeguards equipment, Int. J. Nucl. Energy Sci. Technol. 4 (1) (2008) 72.
[3] T. Honkamaa, F. Levai, A. Turunen, R. Berndt, S. Vaccaro, P. Schwalbach, A Prototype for passive gamma emission tomography, in: IAEA Symposium on International Safeguards: Linking Strategy, Implementation and People, Vienna, 2014.
[4] S. Holcombe, S.J. Svärd, L. Hallstadius, A Novel gamma emission tomography instrument for enhanced fuel characterization capabilities within the OECD Halden Reactor Project, Ann. Nucl. Energy 85 (2015) 837–845.
[5] E.L. Smith, S. Jacobsson, V. Mozin, P. Jansson, E. Miller, T. Honkamaa, et al., Viability Study of Gamma Emission Tomography for Spent Fuel Verification: JNT 1955 Phase I Technical Report, 2016.
[6] E.A. Miller, L.E. Smith, R.S. Wittman, et al., Hybrid Gama Emission Tomography (HGET): FY16 Annual Report NO. PNNL-26213, Pacific Northwest National Lab.(PNNL), Richland, WA United States, 2017.
[7] T.D. Gedeon, D. Harris, Progressive image compression, in: IJCNN International Joint Conference on Neural Networks, 4, 1992.
[8] Y.A. Zhang, Better autoencoder for image: convolutional autoencoder ICONIP17-DCEC, Available from, http://users.cecs.anu.edu.au/Tom.Gedeon/conf/ABCs2018/paper/ABCs2018_paper_58.pdf, 2018.
[9] V.A. Knyaz, O. Vygolov, V.V. Kniaz, Y. Vizilter, V. Gorbatsevich, T. Luhmann, N. Conen, Deep learning of convolutional auto-encoder for image matching and 3d object reconstruction in the infrared range, in: Proceedings of the IEEE International Conference on Computer Vision Workshops, 2017.
[10] L. Gondara, Medical image denoising using convolutional denoising autoencoders, in: 2016 IEEE 16th International Conference on Data Mining Workshops, 2016.
[11] H.J. Choi, I.S. Kang, K.B. Kim, Y.H. Chung, C.H. Min, Optimization of single-photon emission computed tomography system for fast verification of spent fuel assembly: a Monte Carlo study, J. Instrum. 14 (7) (2019) T07002.
[12] L. Rao, B. Zhang, J. Zhao, Hardware implementation of reconfigurable 1-D convolution, Journal of Signal Processing Systems 82 (1) (2016) 1–16.
[13] J. Lemley, S. Bazrafkan, P. Corcoran, Deep Learning for Consumer Devices and Services: pushing the limits for machine learning, artificial intelligence, and computer vision, IEEE Consumer Electronics Magazine 6 (2) (2017) 48–56.
[14] A. Krizhevsky, I. Sutskever, G.E. Hinton, Imagenet Classification with Deep Convolutional Neural Networks. Advances in Neural Information Processing Systems, 2012.
[15] W. Kehl, W. Milletari, F. Tombari, S. Ilic, N. Navab, Deep learning of local RGB-D patches for 3D object detection and 6D pose estimation, in: European Conference on Computer Vision, Springer, Cham, 2016.
[16] O.E. David, N.S. Netanyahu, Deeppainter: painter classification using deep convolutional autoencoders, in: International Conference on Artificial Neural Networks, Springer, Cham, 2016.